Peel Adhesion and Viscoelasticity of Poly(ethylene-*co*-vinyl acetate)-Based Hot Melt Adhesives. II. The Influence of Wax

H.-H. SHIH* and G. R. HAMED

Department of Polymer Science, University of Akron, Akron, Ohio

SYNOPSIS

The influence of wax on the viscoelasticity and peel adhesion of poly(ethylene-*co*-vinyl acetate) (EVA)-based hot melt adhesives was evaluated. Wax does not affect the glass transition temperature of a homogeneous EVA/rosin blend. However, for a heterogeneous EVA/rosin blend, wax addition increases the EVA-rich phase portion, resulting a higher rubbery response. The T-Peel fracture energies of EVA/tackifier/wax blends bonded to polypropylene film are controlled by two factors: (1) a weak boundary layer of wax, which has a deleterious effect on bonding, and (2) on the other hand, an increased rubbery response in the stick-slip region, which tends to strengthen joints.

INTRODUCTION

Hot melt adhesives (HMAs) spread onto substrates in the melt followed by solidification after cooling. Thermoplastics, such as poly(ethylene-*co*-vinyl acetate) (EVA), polyolefins, polyamides, and polyesters, have been the basis of HMAs. A typical EVA-based HMA is formulated with four main components: polymer, tackifier, wax, and antioxidant. The polymer contributes strength and toughness, while tackifier enhances wetting and tack. The wax lowers the melt viscosity and reduces cost. The antioxidant reduces thermal degradation during processing. EVA-based HMAs are widely used in packaging, paper laminating, nonwoven textiles, and book bindings.[1]

Tackifiers and wax are widely used in formulating EVA-based HMAs.[1] Wax has been shown to be deleterious to the adhesion of an EVA HMA without full explanation.[2] Moreover, only a few scientific investigations have been concerned with HMAs.[3,4] In one study,[3] at higher testing temperatures, EVA compositions with 45 wt % rosin and 10 wt % wax had a higher T-Peel strength than did a corresponding composition with resin. The reverse was true at a low testing temperature. In another study,[4] the deleterious effect of wax was attributed to a wax weak boundary layer at the region between the adhesive and the adherend. This was supported by showing that the fractured surface had a low surface tension, like wax. Results of X-ray photoelectron spectroscopy also supported the presence of a weak boundary layer of wax. Unfortunately, the viscoelastic properties of the aforementioned adhesives were not measured in the above two studies, leaving questions concerning how wax affects dynamic properties and how these influence peel strength.

Dynamic mechanical thermal analysis was used to determine how wax affects the viscoelastic properties of model EVA HMAs. Polypropylene (PP) strips were laminated with the adhesives, and T-Peel fracture energies were determined. Finally, correlations between viscoelasticity and peel adhesion are discussed.

EXPERIMENTAL: MATERIALS AND SPECIMENS PREPARATION

Raw materials, including EVA (Escorene 7750; Exxon Company), a hydrogenated rosin ester

* To whom correspondence should be addressed at Union Chemical Laboratory, ITRI, 321 Kung-Fu Road, Section 2, Hsin-Chu, Taiwan, 30042, R.O.C.

Journal of Applied Polymer Science, Vol. 63, 333–342 (1997)
 CCC 0021-8995/97/030333-10

(rosin; Foral 105; Hercules Company), and wax, were combined to give a total batch weight of 45 g. Compositions were melt blended at 120°C for 6 min in a Haake mixer. To reduce thermal degradation, 0.25 parts by weight of antioxidant (Irganox 165; Ciba Geigy Company) was added. Mixtures were compression molded at 120°C for 10 min under 20 tons of force to form sheets 1.5 mm thick.

Samples are designated *E-R-W* $(X : Y)$–Z, where E, R, and W represented EVA and tackifier, and wax, respectively. $X : Y$ is the ratio of EVA to tackifier. Z is the weight fraction of wax, unless 10 wt % of wax is added; then Z is blank. Detailed sample designation and formulations are listed in Table I.

Strips about 5 mm wide were cut, and a Dynamic Mechanical Thermal Analyzer was used to measure viscoelastic properties. The temperature range was −50 to 50°C at an increasing rate of 2°C/min; the frequency was 1 Hz. In order to determine the two glass transition temperatures of a heterogeneous blend, tan δ curves were decomposed by the following methodology. A function representing the tan δ curve is written as

$$F(T) = A_L \exp(-(T - T_{g-L})^2/B_L) + A_H \exp(-(T - T_{g-H})^2/B_H) \quad (1)$$

where A_L and A_H are the peak heights of peaks corresponding to the EVA- and rosin-rich phases, respectively; B_L and B_H are equal to 1.2 times the temperature width at the half-height position of corresponding peak, respectively; T is the temperature; and T_{g-L} and T_{g-H} are the peak temperatures of the peaks corresponding to the EVA- and rosin-rich phases, respectively. First, two numbers representing the two peak temperatures were given and substituted into eq. (1). Then, A_L, A_H, B_L, and B_H were adjusted until the minimum standard error deviation for this pair was reached. Another pair of temperatures was given, and A_L, A_H, B_L, and B_H were obtained again. This trial-and-error was continued, until the smallest standard error deviation was obtained. Thus, the two temperatures giving the best curve fit were assigned as the two glass transition temperatures of the heterogeneous blend. The peak heights also were recorded.

Table I Formulations (Parts by Weight)

	Components			
Sample	EVA	Rosin	Wax	Antioxidant
E-R (8 : 2)	80	20		0.25
E-R-W (8 : 2)	72	18	10	0.25
E-R-W (8 : 2) − 15	68	17	15	0.25
E-R (4 : 6)	40	60		0.25
E-R-W (4 : 6) − 5	38	57	5	0.25
E-R-W (4 : 6)	36	54	10	0.25

An adhesive layer 0.23 mm thick and a 0.16-mm brass spacer were placed between two sheets of PP (0.13 × 200 × 50 mm). The sandwich was placed between two chrome plates and pressed at 120°C and a 3,400 kg/m^2 load for 100 sec with a hot sealer (Sencorp System Inc.). After bonding, the tapes were cooled in air to room temperature. The total thickness of the specimens was 0.42 ± 0.02 mm (with an adhesive thickness of 0.16 ± 0.02 mm). Strips, 25 mm wide and 175 mm long (including 150 mm of bonded PP/HMA/PP and 25 mm of free PP film on one side), were cut for testing. The bond strengths of the laminates were determined in a T-Peel geometry at four temperatures (11, 21, 31, and 41°C) and five rates (5, 20, 50, 200, and 500 mm/min) with an Instron. Peeling energy was determined from the peeling force by the following equation

$$G = 2F/b \quad (2)$$

where G is the peeling energy (N/m); F is the average force required to peel a specimen apart (N); b is width of the test specimen (m). Stick- and slip-band lengths were measured with a traveling microscope. The fractions of stick and slip in a stick-slip cycle also were calculated.

RESULTS AND DISCUSSION

Effect of Wax on Viscoelastic Properties Homogeneous Tackifier/EVA Blend

Previously, it was shown that rosin-tackified EVA (ratio of EVA to rosin is 8 to 2) without wax forms a homogeneous blend. Wax (10 and 15 wt %) was added to this blend and tan δ and E' were measured. Results are shown in Figures 1 and 2. Tan δ peak temperatures did not change with wax addition, but wax lowers peak height and broadens peak width (Fig. 1). As the highly crystalline wax is added to the EVA/rosin blend, crystallinity increases,[5] and therefore, the amorphous volume fraction decreases. It has been proposed that

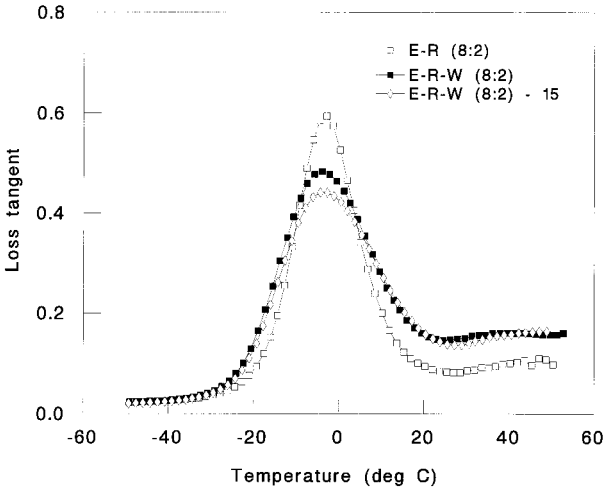

Figure 1 Effect of wax concentration on the loss tangent of E-R (8 : 2).

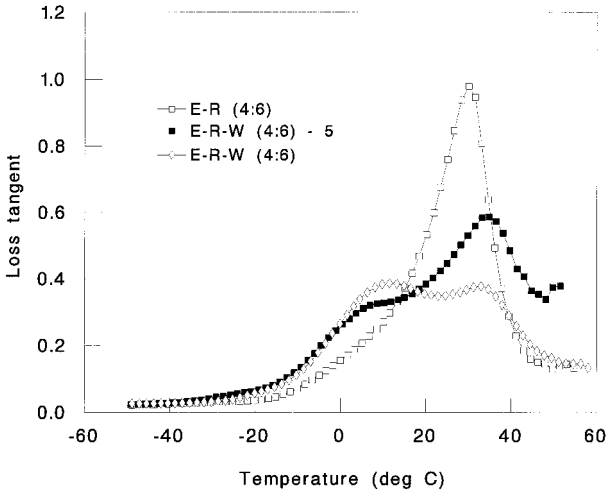

Figure 3 Effect of wax concentration on the loss tangent of E-R (4 : 6).

damping at the glass transition mostly results from segmental motion within the amorphous portion, such that its intensity is proportional to the amorphous volume fraction.[6,7] Thus, wax addition decreases the tan δ peak height. Furthermore, molecular relaxations within amorphous portions of the EVA/rosin/wax adhesive are restricted by added crystallinity, causing a broadening of the tan δ peak.[6,7]

Both E-R-W (8 : 2) and E-R-W (8 : 2)-15 have E' values higher than E-R (8 : 2) (Fig. 2), when the temperature is above their glass transition temperatures. This is attributed to increasing crystallinity.[6,7] However, differences are small in the glassy region.

Summarizing, wax does not affect the glass transition temperature of a homogeneous EVA/rosin blend, but it results in higher crystallinity. The increase in crystallinity causes broadening and lowering of the tan δ peak and enhances the storage modulus.

Effect of Wax on Viscoelastic Properties Heterogeneous Tackifier/EVA Blend

Wax was added to a heterogeneous EVA/rosin blend [E-R (4 : 6)], and viscoelastic properties were determined. Tan δ and E' of E-R (4 : 6), E-R-W (4 : 6)-5, and E-R-W (4 : 6) are shown in Figures 3 and 4. The tan δ peak height and shape

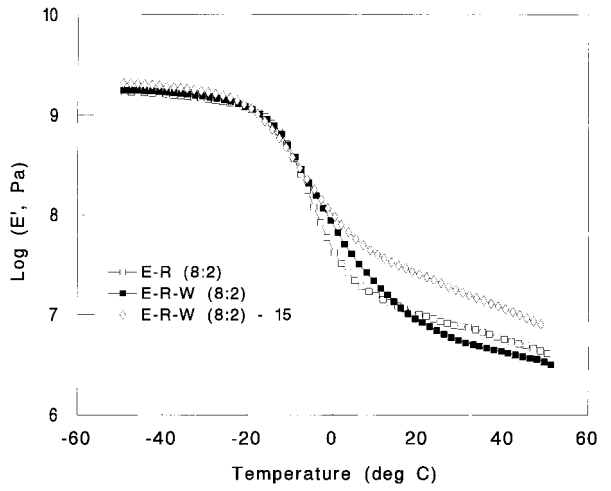

Figure 2 Effect of wax concentration on the storage modulus of E-R (8 : 2).

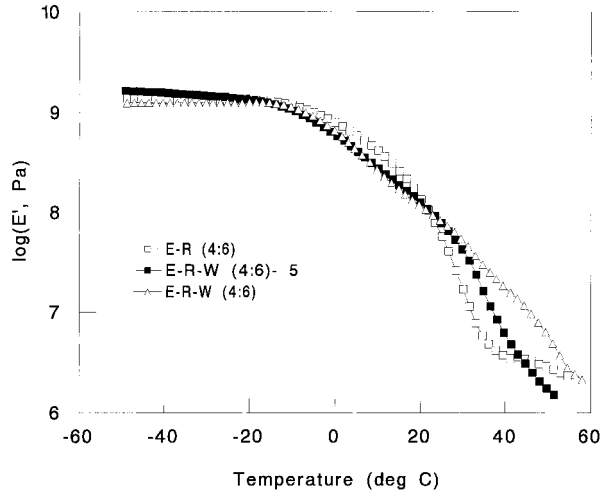

Figure 4 Effect of wax concentration on the storage modulus of E-R (4 : 6).

Table II Tan δ Height and Width, and Glass Transition Temperature of Rosin-Tackified EVA After Decomposition

EVA	$T_{g\text{-}L}$ (°C)	Height	Width (°C)	$T_{g\text{-}H}$ (°C)	Height	Width (°C)
E-R (4 : 6)	15.8	.2942	15.0	30	.8050	8.0
E-R-W (5 : 5) − 5	8	.2079	13.4	30	.5113	14.3
E-R-W (5 : 5)	7.5	.2888	13.9	31.9	.3274	16.1

change with increasing wax concentration (Fig. 3). To further analyze the results, the tan δ curves were decomposed. Glass transition temperatures and peak heights corresponding to both EVA-rich and rosin-rich phases are listed in Table II and Figures 5 and 6. The results suggest that all four samples are heterogeneous, because the shapes of the tan δ peaks continuously change with increasing wax concentration. Wax addition has little effect on T_{g-H} but decreases the T_{g-L}. The height of the T_{g-H} peak declines with increasing wax concentration, but the height of the T_{g-L} peak changes little with wax addition. A possible explanation follows.

As wax is added to the rosin-tackified EVA, it may enhance EVA/rosin compatibility. As the EVA/rosin compatibility increases, the EVA and rosin prefer to stay at the composition where the rosin and EVA are more compatible, such as 30 wt % rosin. This causes the EVA and rosin to diffuse from the rosin-rich domains and enter the EVA-rich domains. Thus, the concentration of the EVA-rich domain increases, and the composition of EVA-rich domain decreases. The composition of rosin-rich domains may keep constant while the concentration decreases. This explains why wax addition has little effect on T_{g-H} but decreases the T_{g-L}. Also, as noted before, wax lowers the tan δ peak intensity. These two effects causes the peak height of T_{g-H} to decrease with wax concentration. However, a different trend can be seen in the EVA-rich phase. Wax addition increases the concentration of the EVA-rich phase, resulting in a larger relaxation intensity (i.e., peak height increases). At the same time, wax decreases peak height. Thus, the tan δ peak intensity of the EVA-rich phase is a compromise between these two contradictory effects. This is why the height of the T_{g-L} peak changes little with wax addition.

The storage moduli of the three adhesives are given in Figure 4. In order to discern these more clearly, results are compared in pairs. The storage moduli of E-R (4 : 6) and E-R-W (4 : 6) are shown in Figure 7. The storage modulus of E-R-W (4 : 6) is higher than that of E-R (4 : 6) when the temperature is between 22 and 53°C. There is a slight reversal below 22°C. In the glassy state, the two are indistinguishable. Similar trends were observed when comparing E-R (4 : 6) with E-R-W (4 : 6) − 5 (Fig. 4). As described before, wax enters both phases and changes relative EVA- and

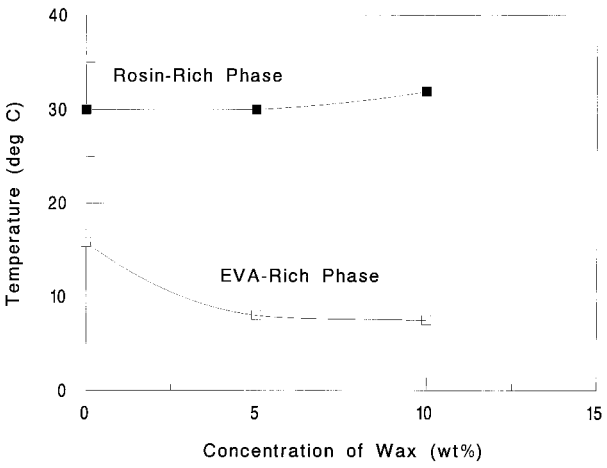

Figure 5 Effect of wax concentration on the glass transition temperature of E-R (4 : 6).

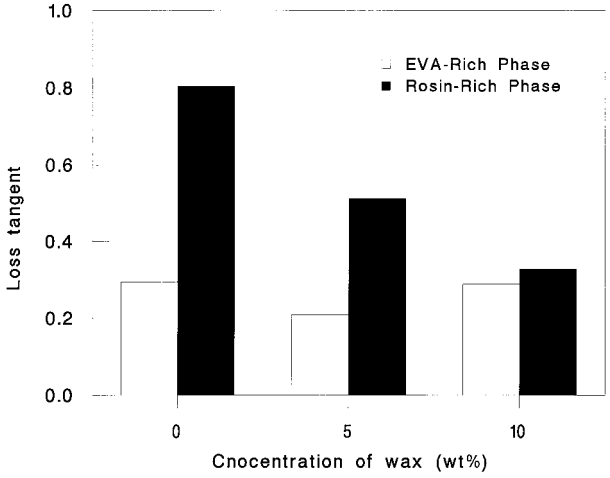

Figure 6 Effect of wax concentration on the loss tangent peak height of E-R (4 : 6).

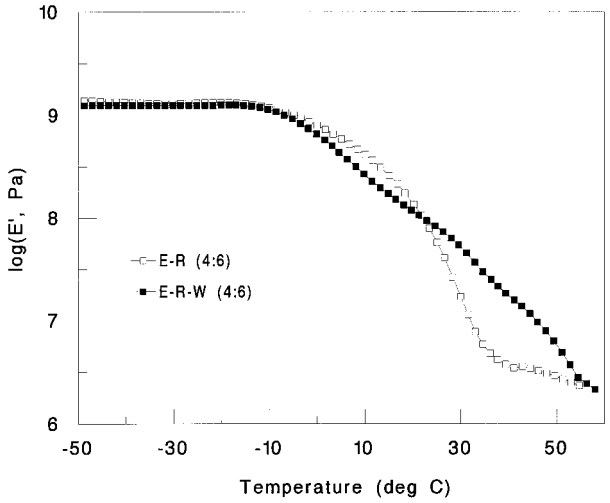

Figure 7 Storage modulus of E-R (4 : 6) and E-R-W (4 : 6).

rosin-rich phase concentrations. The reinforcing effect of the glassy rosin-rich domain on the rubbery EVA-rich domain is less without wax. At the same time, the higher concentration of the EVA-rich phase increases the rubbery response of the adhesive containing wax. This influence results from a change in phase concentrations. Moreover, as wax enters the EVA- and rosin-rich phases, the moduli of both the EVA- and the rosin-rich domains increase. The storage moduli of EVA/rosin adhesives with wax are controlled by concentration variations resulting in more rubbery (from the EVA-rich phase) and less glassy (from the rosin-rich phase) contributions to the bulk storage modulus, thereby, depressing the storage modulus. On the other hand, higher crystallinity with wax enhances the storage modulus of both phases. When the temperature is higher than the glass transition temperature of the rosin-rich phase, adhesives with and without wax are in the rubbery state. The later contribution, then, will control the storage modulus; i.e., wax addition increases storage modulus. It seems that the former contribution becomes important, when the temperature is just below the glass transition temperature of the rosin-rich phase. This explains why the rosin-tackified adhesive with wax has higher E' than that without wax. Furthermore, this wax-induced concentration change, resulting in lower E', becomes increasingly important, as temperature further decreases.

The storage moduli of E-R-W (4 : 6) − 5 and E-R-W (4 : 6) are also shown in Figure 4. The storage moduli of rosin-tackified EVA with more wax are higher than those with less wax at temperatures above T_{g-H} or below T_{g-L}. The opposite is true at the interval between the two glass transition temperatures.

Wax addition has a complex influence on the viscoelastic properties of tackified EVA. For a homogeneous EVA/rosin blend, wax has little effect on the glass transition temperature and lowers and broadens the tan δ peak, as well as enhancing the storage modulus at temperatures above their glass transitions. However, for heterogeneous EVA/rosin blends, wax addition shows more complicated effects. Wax increases the EVA-rich phase portion and decreases the rosin-rich phase.

Observations of T-Peel Fracture Behavior

Several different failure modes were observed in T-Peel testing: (1) interfacial, (2) cohesive, (3) stick-slip, and (4) mixed mode. Interfacial failure occurs between the PP and the adhesive. This fracture has been attributed to the adhesive being in its rubbery state.[8] When a specimen is peeled, the adhesive detaches from the adherend, leaving no residue on the PP surface.

Cohesive failure is fracture occurring within the adhesive layer; a typical fracture surface is shown in Figure 8. The predominant viscoelastic response of the adhesive is viscous flow.[8] When the adhesive is subjected to a peeling force, it is deformed. U- or V-shaped holes, with tips opposite to the peeling direction, form. When cohesive failure and interfacial failure occur simultaneously, this is called cohesive-interfacial failure or mixed-mode I.

When stick-slip fracture occurs, the peel force alternates between an initiation (peak) and an arrest value.[8] Failure occurs at the interface between the adhesive and the PP in both the stick

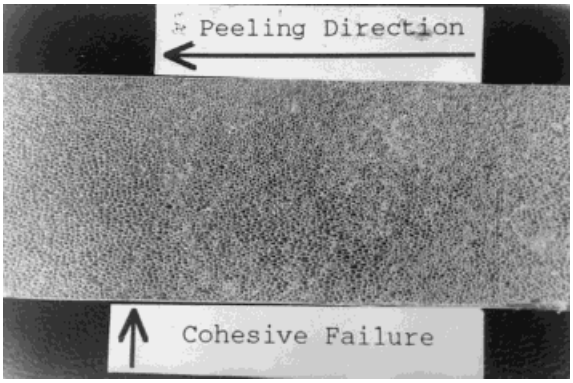

Figure 8 Fracture surface for cohesive failure.

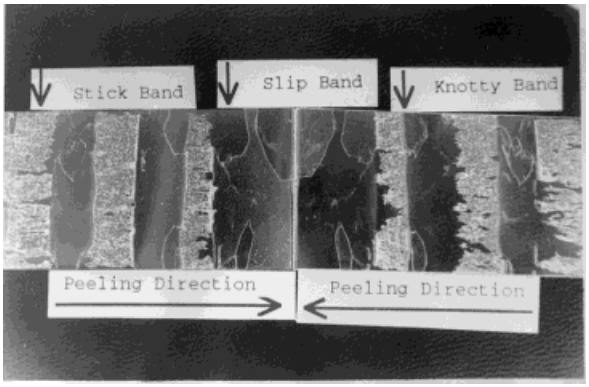

Figure 9 Fracture surface for mixed-mode II.

and the slip regions. Transparent bands with smooth surfaces are found where rapid, slip-fracture occurred. Translucent bands with rough surfaces appear where slower, stick-fracture occurred. This failure has been attributed to the adhesive alternating between rubbery and glassy responses.[8] At the onset of the stick behavior, crack growth slows and the force increases rapidly. Elastic energy is stored in the unattached strip. Peeling remains stable if the stored elastic energy does not exceed a critical value. If exceeded, rapid peeling ensues. The rapid peeling continues until the excessive energy is expended and the force falls below a critical value. Here, the energy is insufficient to sustain such a high peeling rate, and the crack speed reverts to the original slow rate. This completes a cycle of "stick-slip" oscillation.

Mixed-mode II is stick-slip with interfacial-cohesive failure in the stick region, preceded by a knotty band and relatively brittle fracture in the slip interval. A representative fracture surface is shown in Figure 9. At the onset of the stick region, a crack occurs between the adhesive and the PP film. It propagates along the peeling direction for a short distance; then, the crack deviates into the adhesive layer nearly perpendicular to the peeling direction. It then propagates back toward the interface and meets the interface at a position slightly advanced from where the crack penetrated the adhesive layer. An adhesive band and a V-shaped groove can be seen on the PP film and on the adhesive side, respectively. This is called a knotty band. In this region, the crack growth rate is slow and the T-Peel force increases much slower than that in the stick region, where stick-slip occurred. This results in a broader peel force peak. After the peel force reaches a maximum, a mixed cohesive-interfacial failure is observed in the remaining stick region. Crack growth remains slow, and the T-Peel force, with some minor fluctuations, stays at a nearly constant peak value. As slip is initiated, the crack propagates very quickly along the peeling direction and the stored elastic energy is released in a short period. Fracture mainly occurs between the adhesive and the PP. The degree of brittleness depends on the testing rate and temperature. If peeling is conducted at a high rate, new fracture surfaces may be found, either at the same interface as in the stick region or at the opposite one, due to the adhesive fracturing cohesively, thereby causing the crack to shift to the other interface. Thus, cracks may propagate at two interfaces, forming flake-like pieces. As peeling rate decreases, brittle fracture is reduced and eventually eliminated.

Mixed-mode III (Fig. 10) is stick-slip having a leading knotty band, followed with or without an interfacial failure band in the remaining stick region and an interfacial failure in the slip interval. The crack propagation behavior is similar to that of mixed-mode I, except interfacial-cohesive failure and brittle failure are not seen. Mixed-mode IV is stick-slip failure where a cohesive-interfacial failure occurs in the stick region and interfacial failure occurs in the slip interval.

T-Peel Strength of E-R (4 : 6) and E-R-W (4 : 6)

T-Peel fracture energies for E-R (4 : 6) and E-R-W (4 : 6) tested at 11°C and five peeling rates are plotted in Figure 11. Random interfacial failure was observed for E-R (4 : 6) at five peeling rates. Below 200 mm/min peeling rate, stick-slip was observed for the E-R-W (4 : 6), while random interfacial failure was observed for other peeling rates.

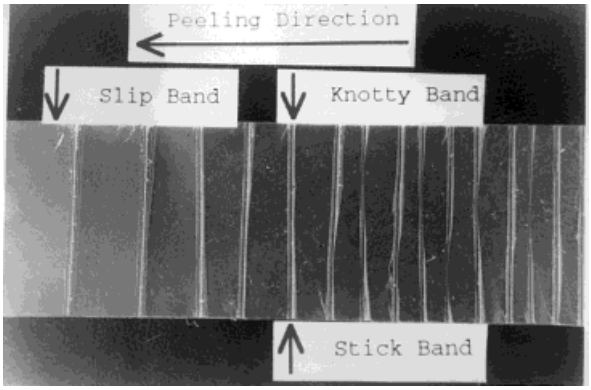

Figure 10 Fracture surface for mixed-mode III.

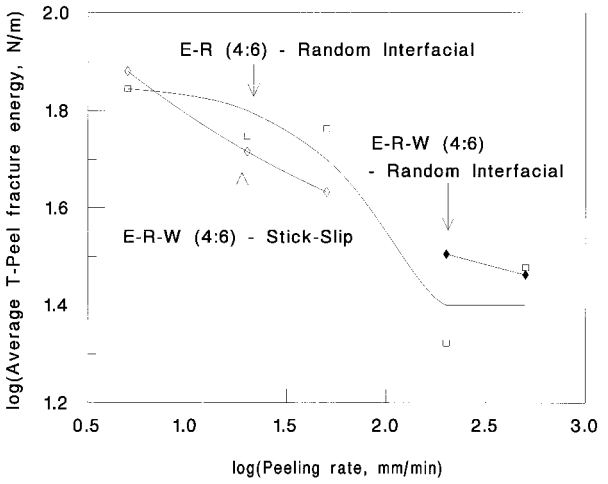

Figure 11 Average T-Peel fracture energies of E-R (4 : 6) and E-R-W (4 : 6), measured at 11°C.

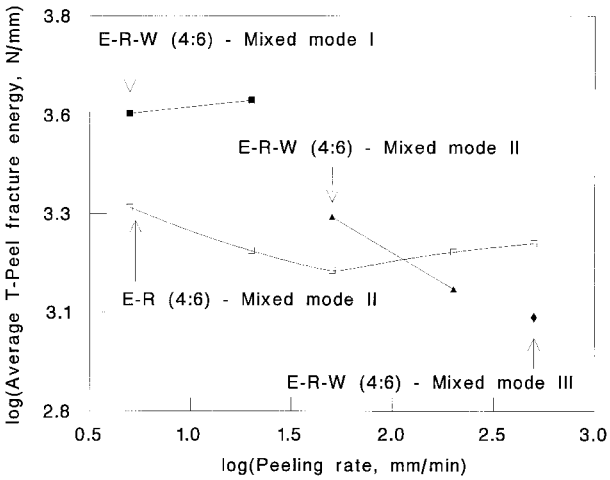

Figure 13 Average T-Peel fracture energies of E-R (4 : 6) and E-R-W (4 : 6), measured at 31°C.

T-Peel fracture energies for E-R (4 : 6) and E-R-W (4 : 6) tested at 21°C are plotted against peeling rate in Figure 12. Stick-slip failure was observed for E-R-W (4 : 6) at all rates and for E-R (4 : 6) when the peeling rates are at 500, 200, and 50 mm/min. Mixed-mode III failure was observed at lower peeling rates for E-R (4 : 6). At 5 mm/min, E-R (4 : 6) has T-Peel average fracture energies similar to those of E-R-W (4 : 6). However, as the peeling rate increases, the T-Peel average fracture energies for E-R-W (4 : 6) become higher than those for E-R (4 : 6).

Figure 13 shows fracture energies for E-R (4 : 6) and E-R-W (4 : 6) peeled at 31°C. Mixed-mode II failure is observed for E-R (4 : 6). However, the failure mode for E-R-W (4 : 6) shifted from mixed-mode I to mixed-mode II to mixed-mode III as peeling rate increased. T-Peel fracture energies for E-R-W (4 : 6) are higher than those for E-R (4 : 6) below 50 mm/min, while the opposite is observed at other peeling rates.

T-Peel fracture energies for E-R (4 : 6) and E-R-W (4 : 6) peeled at 41°C are plotted against peeling rate in Figure 14. Below 200 mm/min, cohesive failure was observed for E-R (4 : 6) and E-R-W (4 : 6). When peeling rate is increased to 500 mm/min, the failure modes of E-R-W (4 : 6) and E-R (4 : 6) shift to mixed-mode IV and I, respectively. At 500 mm/min, the average T-Peel fracture energy for E-R (4 : 6) is smaller than that for E-R-W (4 : 6) with mixed-mode IV. E-R-W

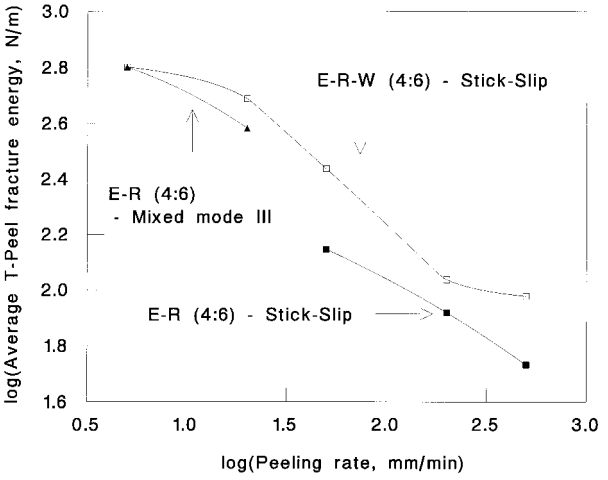

Figure 12 Average T-Peel fracture energies of E-R (4 : 6) and E-R-W (4 : 6), measured at 21°C.

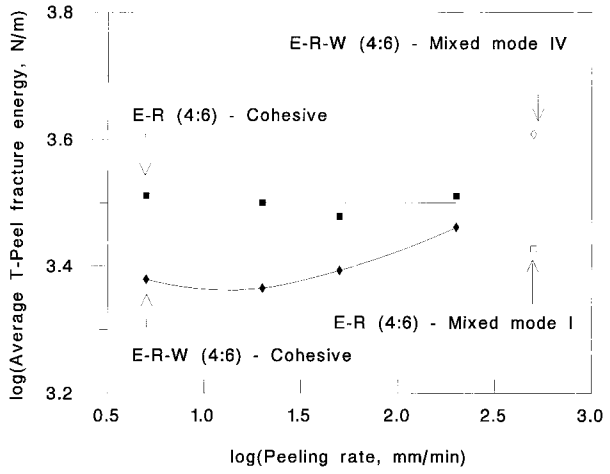

Figure 14 Average T-Peel fracture energies of E-R (4 : 6) and E-R-W (4 : 6), measured at 41°C.

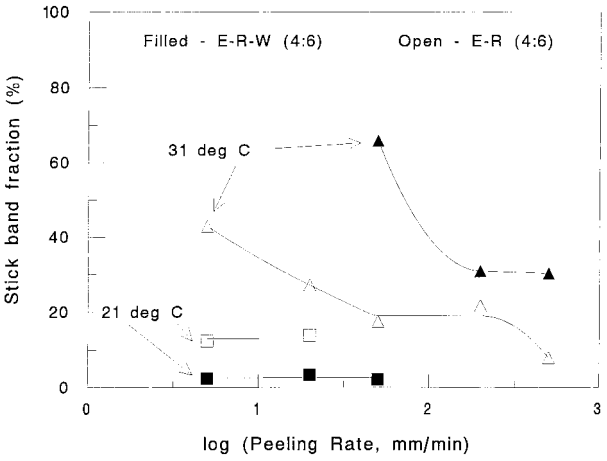

Figure 15 Stick-band fraction of E-R (4 : 6) and E-R-W (4 : 6), tested at 21 and 31°C.

(4 : 6) has a lower average fracture energy than does E-R (4 : 6) at the other four peeling rates.

Stick-band fractions for E-R (4 : 6) and E-R-W (4 : 6) are shown in Figure 15. Failure modes are listed in Table III. At 11°C, stick-bands are too small to be observed by microscopy; thus, the stick-band fraction cannot be calculated. The stick-band fraction for E-R-W (4 : 6) is about 2% at 21°C, while that for E-R (4 : 6) is about 14%. The stick-band fraction for E-R (4 : 6) and E-R-W (4 : 6) at higher peeling rates cannot be measured because it is too small. For E-R (4 : 6), mixed-mode III was observed. Knotty band fractions in the stick-band region are 50 and 20% at 5 and 20 mm/min, respectively.

When testing temperature increases to 31°C, mixed-mode II with complex fracture surfaces was observed for E-R (4 : 6). The fracture surfaces are described and the fractions of each fracture mode are listed in Table IV. Stick-band fractions for E-R (4 : 6) decrease initially, reach a plateau, and then decrease again with a further increase in peeling rate. A similar trend is observed for E-R-W (4 : 6), except that the stick-band fraction did not further decrease at higher peeling rates. Below a peeling rate of 200 mm/min, mixed cohesive and interfacial failure, with a leading knotty band, can be observed in all stick regions. The knotty band fraction in a stick-band decreases with increasing peeling rate, while the mixed-mode fraction decreases. The cohesive failure fraction in the mixed region decreases with increasing peeling rate, and the interfacial failure fraction in the mixed region increases with increasing peeling rate. The area fraction of knotty bands in the stick-bands increases with increasing peeling rate, while the area of interfacial and cohesive band fraction decreases. At 500 mm/min, mixed-mode failure with a leading knotty band could only be seen in 90% of the stick-bands. Interfacial failure is seen in the other stick-bands. The fraction of knotty, interfacial, and cohesive failure is similar to those for E-R (4 : 6) at 500 mm/min. For E-R-W (4 : 6), the failure mode changes with increasing peeling rate. Fracture surfaces are described and the fractions of each fracture mode are listed in Table V. At lower peeling rates, the area fraction of cohesive failure and interfacial failure remains constant. These are about 82.5 and 17.5%, respectively. At a peeling rate of 500 mm/min, mixed-mode III failure, having 100% of knotty band in the stick region, is seen. This further shows that the rubbery response of the adhesive decreases with increasing peeling rate.

When testing temperature increases to 41°C, mixed-mode I with 80% cohesive failure and mixed-mode IV with 90% cohesive failure were

Table III Failure Modes of PP/E-R (4 : 6) and E-R-W (4 : 6)/PP Tested at Various Temperatures and Peeling Rates

Peeling Rates (mm/min)	E-R-W (4 : 6) at (°C):				E-R (4 : 6) at (°C)			
	11	21	31	41	11	21	31	41
5	SS	SS	M1	C	RI	M3	M2	C
20	SS	SS	M1	C	RI	M3	M2	C
50	SS	SS	M2	C	RI	SS	M2	C
200	RI	SS	M2	C	RI	SS	M2	C
500	RI	SS	M3	M4	RI	SS	M2	M1

SS, C, RI, M1, M2, M3, and 4 represent the stick-slip, cohesive, random interfacial, mixed-mode I, mixed-mode II, and mixed-mode III, and mixed-mode IV, respectively.

Table IV Area Fractions of Various Failure Modes in the Stick-Band Region for E-R (4 : 6) Tested at 31°C

Peeling Rate (mm/min)	f_K	f_{MDI}	f_C	f_I	$f(A)_k$	$f(A)_I$	$f(A)_C$
5[a]	10	90	85	15	10	13.5	76.5
20[a]	50	50	70	30	50	15	35
50[a]	80	20	20	80	80	16	4
200[a]	90	10	30	70	90	7	3
500[b]	78	22	30	70	78	15.4	6.6

f_K and f_{MDI} are the knotty band fraction and the mixed-mode band fraction in the stick band, respectively. f_C and f_I are the fraction of cohesive and interfacial failure in the mixed-mode failure region, respectively. $f(A)_K$, $f(A)_I$, and $f(A)_C$ are area fraction of knotty, interfacial, and cohesive failure in the stick band, respectively.

[a] All stick bands show mixed-mode failure.

[b] Ten percent of stick band shows interfacial failure, and the others show mixed-mode failure.

observed for E-R (4 : 6) and E-R-W (4 : 6), respectively, at 500 mm/min. For other peeling rates, cohesive failure was observed for the two adhesives.

Correlation Between T-Peel Strength and Viscoelastic Properties

From the variations of the stick-band fractions and fracture modes for E-R (4 : 6) and E-R-W (4 : 6), the following conclusion are drawn. First, the addition of wax increases the stick-band fraction, indicating that the rubbery response increases from this addition (Fig. 15). Next, the early appearance of mixed-mode I (cohesive with adhesive failure) for E-R-W (4 : 6), as shown at lower peeling rates at 31°C and for 500 mm/min at 41°C, suggests that E-R-W (4 : 6) meets its critical viscous response earlier than does E-R (4 : 6). Third, for E-R (4 : 6), the failure region (interfacial failure) representing the glassy response disappeared at a higher temperature, as a result of the more glassy response of E-R (4 : 6). Also, the stick-slip region is narrowed as wax is added to the rosin-tackified EVA. Finally, wax lowers the area fraction representing the rubbery or viscous response from the adhesive. This evidence further supports the hypothesis made in the previous section. In other words, wax enhances the compatibility between EVA and tackifier, resulting in a higher concentration of the more stable EVA-rich phase and a more rubbery response during peeling.

At 41°C, the T-Peel strength with cohesive failure for E-R (4 : 6) is higher than that for E-R-W (4 : 6) with the same failure mode. This is because the addition of wax decreases the viscosity of the rosin-tackified EVA.[5] Thus, a lower force is needed to deform and pull out chains.

It is quite surprising that E-R-W (4 : 6) has a higher T-Peel strength than E-R (4 : 6) at 21°C. It has been shown that wax lowers the bond strength of an EVA/tackifier adhesive as the result of a weak boundary layer.[3] It is expected, then, that E-R (4 : 6) will have the higher bond

Table V Area Fractions of Various Failure Modes in the Stick-Band Region for E-R-W (4 : 6) Tested at 31°C

Peeling Rate[a] (mm/min)	f_K	f_{MDI}	f_C	f_I	$f(A)_k$	$f(A)_I$	$f(A)_C$
5						15	85
20						20	80
50	10	90	90	10	10	9	81
200	75	25	70	30	75	7.5	17.5
500	100				100		

f_K and f_{MDI} are the knotty band fraction and the mixed-mode band fraction in the stick band, respectively. f_C and f_I are the fraction of cohesive and interfacial failure in the mixed-mode failure region, respectively. $f(A)_K$, $f(A)_I$, and $f(A)_C$ are area fraction of knotty, interfacial, and cohesive failure in the stick band, respectively.

[a] All stick bands show mixed-mode failure.

strength. However, there is an opposing effect—wax induces a more rubbery response, resulting in a higher bond strength. At the five peeling conditions, a wax-enhanced, more rubbery response, resulting in higher T-Peel strength, may overcome the deleterious effect of a wax weak boundary layer. This explains why the T-Peel force of E-R (4 : 6) is lower than that of E-R-W (4 : 6).

When samples were tested at 31°C and a low peeling rate, the T-Peel force for E-R (4 : 6) was lower than that for E-R-W (4 : 6). The trend is similar to that found at 21°C; thus, similar reasoning can be used to explain the phenomena. At a higher peeling rate, the rubbery response becomes progressively smaller, as shown by the decrease of area fraction representing the viscous and rubbery responses in the stick region. This results in a smaller increase in T-Peel strength. Thus, the wax weak boundary layer dominates the wax-induced-rubbery response. This is why E-R (4 : 6) has a higher T-Peel strength than E-R-W (4 : 6).

Wax addition increases and decreases EVA- and tackifier-rich phase concentrations of a heterogeneous blend, respectively. Moreover, the T-Peel strengths of the EVA/tackifier/wax adhesives are controlled by the wax weak boundary layer and the extent of rubbery response during testing. The former harms the T-Peel strength, while the later has the opposite effect.

CONCLUSION

Wax induces a complex influence on the viscoelastic properties of tackified EVA. Wax has little effect on the glass transition temperature of a homogeneous EVA/rosin blend; it broadens and lowers the tan δ peak and also enhances the storage modulus at temperatures above their glass transitions. For heterogeneous EVA/rosin blends, wax addition increases and decreases EVA- and tackifier-rich phase concentrations, respectively. Above the glass transition temperatures, wax induces more rubbery responses, leading to a lower storage modulus. Moreover, the T-Peel strengths of the EVA/tackifier/wax adhesives are controlled by the wax weak boundary layer and the extent of rubbery response during testing. The former harms the T-Peel strength, while the latter has the opposite effect.

One of the authors (H.-H.S.) gratefully acknowledges the Industry Technology Research Institute (ITRI), Taiwan, R.O.C., for the continuous financial support during his study at the University of Akron. The authors also thank the Exxon and Hercules companies for their support. Many thanks go to Mr. Chung-Sea Shen for his help in decomposition software.

REFERENCES

1. E. F. Eastman and L. Fullhart, Jr., in *Handbook of Adhesives,* I. Skeist, Ed., Van Nostrand Reinhold, New York, 1990.
2. J. D. Domine, and R. H. Schaufelberger, in *Handbook of Adhesives,* I. Skeist, Ed., Van Nostrand Reinhold, New York, 1977.
3. M. F. Tse, L. Hendewerk, K. O. McElrath, and M. Faissat, *The Adhesion Society Proceedings of the Fourteenth Annual Meeting,* 161-3.9(12)4. Feb. 17–20, 1991.
4. A. S. Tathgur, thesis, University of Akron, Akron, Ohio, 1991.
5. Hsi-Hsin Shih, dissertation, University of Akron, Akron, Ohio, 1993.
6. L. E. Nielsen, *Mechanical Properties of Polymers and Composites,* Vol. 1, Marcel Dekker, New York, 1974.
7. M. Takayuki, *Dynamic Mechanical Analysis of Polymeric Materials,* Elsevier North-Holland, New York, 1978.
8. A. N. Gent and A. J. Kinloch, *J. Polym. Sci. A-2.,* **9,** 659 (1971).

Received March 13, 1996
Accepted July 27, 1996